

# The ICON project: development of a unified model using triangular geodesic grids

**Luca Bonaventura**

*Max Planck Institut für Meteorologie  
Hamburg, Germany  
bonaventura@dkrz.de*

## ABSTRACT

An overview of the ICON project for the development of a nonhydrostatic GCM based on triangular geodesic grids is presented. The main motivations, targets and features of the new model are outlined. The horizontal discretization approach is introduced, in the context of the shallow water model developed during the preliminary phase of the project. Numerical results obtained with the shallow water model are presented, showing that the proposed approach allows for accurate simulation of the main features of large scale atmospheric flows. The main open issues regarding the future model development are reviewed.

## 1 Introduction

ICON (acronym for ICOSahedral Nonhydrostatic) is a joint project of the Max Planck Institute of Meteorology Hamburg (MPIfM) and Deutscher Wetterdienst (DWD), the weather forecasting service of Germany, for the development of a new general circulation model. The project target is a unified model for global and regional climate simulation and weather forecasting. The new model will be based on finite volume discretizations of the fully elastic, nonhydrostatic Navier-Stokes equations on geodesic, icosahedral, locally refinable grids. Various research institutes in Germany and elsewhere are also contributing to the project, among which PIK Potsdam, Freie Universität Berlin, AWI Bremerhaven, the Max Planck Institut for Computer Science in Saarbrücken and Colorado State University.

A number of reasons have lead to the choice of reshaping thoroughly the presently available models. Recent investigations (see e.g. [19]) have shown the problems arising when the spectral transform method is coupled to conservative, monotonic advection of tracers by finite volume schemes, among which some major inaccuracies in the simulation of troposphere - stratosphere tracer exchange. These problems are related to the lack of *consistency with the discrete continuity equation*, a concept whose relevance has been discussed in various recent studies on conservative advection schemes (see e.g. [20], [21], [31]). It is easy to show that the discrepancy between the discretization of the divergence term in the continuity equation and in the tracer equations leads to an effective violation of mass conservation and monotonicity of tracer concentrations, even when flux form monotonic schemes are employed (see e.g. [14]). Possible fixes either do not solve the problem effectively or increase significantly the computational cost, if e.g. consistent velocity fields have to be computed on a finite difference grid by an *a posteriori* least squares fit.

Another key issue is regionalization of climate and NWP models. Most nesting approaches currently implemented require strong smoothing at the boundaries of refined areas, because of inappropriate treatment of the internal grid boundaries. The resulting models are not mass conservative and often display unphysical vertical velocities and precipitation patterns at the boundaries. This contrasts with the great accuracy in the treatment

of internal grid interfaces that has been achieved by fully conservative local grid refinement approaches developed over the last 20 years in the CFD community, along with efficient solvers to handle elliptic problems on locally refined grids and efficient dynamically adaptive algorithms (see e.g., among many others, [1], [4], [8], [9], [12], [20]). The development of accurate models for geophysical flows that incorporate these features appears rather attractive because of the potential gain in accuracy, efficiency and flexibility.

From a more practical point of view, both MPIfM and DWD maintain up to now separate models for global and regional simulations, which entails unavoidable overhead and special interfaces for data exchange between the different models. The global and regional model of DWD are even using completely different grids and data structures and special interpolation operators are required to provide the boundary conditions to the regional model.

The main features of the envisaged model formulation will be presented in sections 2 to 4. The horizontal discretization approach will be presented in the context of a semi-implicit, mass and vorticity preserving shallow water model that has been developed as a preliminary step towards the full three dimensional model. Numerical results obtained so far with this model are reported in section 5 and some of the main open issues regarding the future model development are discussed in section 6.

## 2 The model equations

The model under development in the ICON project will use the fully elastic, nonhydrostatic Navier-Stokes equations, which provide a framework that is sufficiently general for meteorological applications on most scales relevant for numerical weather prediction and climate simulation. A formulation of the basic dynamical equations of motion of dry air in the inviscid case which appears to have some advantages is the following:

$$\frac{\partial \rho}{\partial t} + \nabla \cdot (\rho \mathbf{v}) = 0 \quad (1)$$

$$\frac{\partial \mathbf{v}}{\partial t} = -\nabla K - (2\boldsymbol{\Omega} + \boldsymbol{\zeta}) \times \mathbf{v} - \frac{1}{\rho} \nabla \cdot p + \nabla \Phi + \mathbf{F}, \quad (2)$$

$$\frac{\partial (\rho \varepsilon)}{\partial t} + \nabla \cdot [(\rho \varepsilon + p + \mathbf{R}) \cdot \mathbf{v}] = 0 \quad (3)$$

Here,  $\mathbf{v}$  denotes the velocity of dry air, which is interpreted as the baricentric velocity of the dry air components, thus allowing for a rigorous derivation of the energy balance.  $\varepsilon$  is the total energy,  $K$  is kinetic energy,  $\boldsymbol{\Omega}$  denotes the rotation velocity of the Earth,  $\boldsymbol{\zeta} = \nabla \times \mathbf{v}$  is the relative vorticity,  $\Phi$  denotes the normal gravity potential,  $\mathbf{F}$  denotes the resultant of the external forces,  $\mathbf{R}$  denotes the radiation heat flux. This set of equations has to be supplemented by conservation laws for the various (dry and moist) air components, chemical species and ions. This formulation would allow for application of momentum advection schemes without spurious vorticity production (see e.g. [22] and section 4) and for total energy conservation. Relevant issues for the final choice will be the concurrently designed treatment of the moist species and the need for a formulation that is practical for semi-implicit time discretization. It is planned to use height based, terrain following  $\sigma$  as a vertical coordinate. It is also planned to develop a hydrostatic model as an intermediate step, employing the more standard set of primitive equations and hybrid pressure vertical coordinate as for example in the ECHAM5 model [28], [29], so as to assess the impact of a new horizontal discretization on the existing physical parameterizations. For the purpose of developing and testing the horizontal discretization, the vector

invariant form of the shallow water equations on the sphere has been considered:

$$\frac{\partial \mathbf{v}}{\partial t} = -(\zeta + f)\mathbf{k} \times \mathbf{v} - \nabla(gh + K), \quad (4)$$

$$\frac{\partial h}{\partial t} + \nabla \cdot (h^* \mathbf{v}) = 0, \quad (5)$$

$$\frac{\partial(ch^*)}{\partial t} + \nabla \cdot (ch^* \mathbf{v}) = 0. \quad (6)$$

Here  $\mathbf{v} = (u, v)$  is the horizontal velocity vector (on the sphere),  $K = \frac{1}{2}(u^2 + v^2)$  is the kinetic energy,  $\zeta$  is the vertical component of the relative vorticity,  $f$  is the Coriolis coefficient,  $h^*$  is fluid depth,  $h = h^* + h_s$  is the height of the free surface above mean sea level,  $h_s$  is the height of the orography,  $g$  is the gravitational constant and  $\mathbf{k}$  the unit vector in the radial outward direction. Equation (6) is the conservation law for a generic tracer of concentration  $c$ , which is also included in order to stress some basic requirements of its flux form discretization. Furthermore, taking the curl of equation (4) yields the vorticity equation

$$\frac{\partial \zeta}{\partial t} + \nabla \cdot ((\zeta + f)\mathbf{v}) = 0. \quad (7)$$

### 3 The discretization grid and the discrete operators

The proposed discretization method is defined for concreteness on a special case of Delaunay triangulation on the sphere, i.e. the icosahedral geodesic grid, which provides a quasi-uniform coverage of the sphere and displays a hierarchical structure that can be exploited for local grid refinement on nested grid hierarchies. Finite element approaches based on such geodesic grids have been introduced in [3],[10], [13],[17]. Finite volume approaches were instead presented in [16], [26], [27]. Although we will only refer to the icosahedral grid in the following, it is easy to see that the method can be easily generalized to more general Delaunay triangulations, under mild regularity assumptions (see e.g. [23]). The icosahedral construction yields a Delaunay triangulation of the sphere to which a Voronoi tessellation is naturally associated (see e.g. [11] and the references therein for a complete description of Delaunay-Voronoi grid pairs on the sphere), which consists of convex spherical polygons (either pentagons or hexagons, see figure 1).

Some notation to describe the grid topology and geometry will now be introduced. Let then  $i$  denote the generic cell of the Delaunay grid. Let  $\mathcal{E}(i)$  denote the set of all edges of cell  $i$  and  $\mathcal{C}(i)$  the set of all cells which have edges in common with cell  $i$ . The gridpoint associated to cell  $i$  will also be referred to as the cell center. The generic vertex of a cell, which is also the center of a cell in the dual grid, is denoted by  $v$ .  $\mathcal{C}(v)$  denotes the set of all cells of which  $v$  is a vertex and  $\mathcal{E}(v)$  denotes the set of all edges of the dual cell whose center is vertex  $v$ . The area of cell  $i$  is denoted by  $A_i$ , while the area of the dual cell is denoted by  $A_v$ . Let then  $l$  denote the generic edge of a cell. The length of the edge  $l$  of a cell is denoted by  $\lambda_l$  and the distance between the centers of the cells adjacent to edge  $l$  (i.e., the length of a edge of the dual cell) is denoted by  $\delta_l$ . At each edge, a unit vector  $\mathbf{N}_l$  normal to the edge  $l$  is assigned.  $\mathbf{T}_l$  denotes the unit vector tangential to the edge  $l$ , chosen in such a way that  $\mathbf{N}_l \times \mathbf{k}_l = \mathbf{T}_l$  holds, where  $\mathbf{k}_l$  denotes the radial outgoing unit vector perpendicular to the tangent plane at the intersection of primal and dual edge  $l$ . Furthermore, for each cell edge, the unit vector pointing in the outer normal direction with respect to cell  $i$  is denoted by  $\mathbf{n}_{i,l}$ . Unit vectors  $\mathbf{n}_{v,l}$  are also introduced, as pointing in the outer normal direction with respect to the dual cell  $v$ . The corresponding tangential vectors  $\mathbf{t}_{v,l}$  are defined so that  $\mathbf{n}_{v,l} \times \mathbf{t}_{v,l} = \mathbf{k}_l$ . It can be seen that, by simple geometric arguments, one has  $\mathbf{N}_l \cdot \mathbf{t}_{v,l} = \mathbf{T}_l \cdot \mathbf{n}_{v,l}$ .

In order to develop an analog of the rectangular C-type staggering (see e.g. [2]) on the Delaunay grids, the *mass points* are defined as the centers of the grid cells, while the *velocity points* are defined for each cell edge

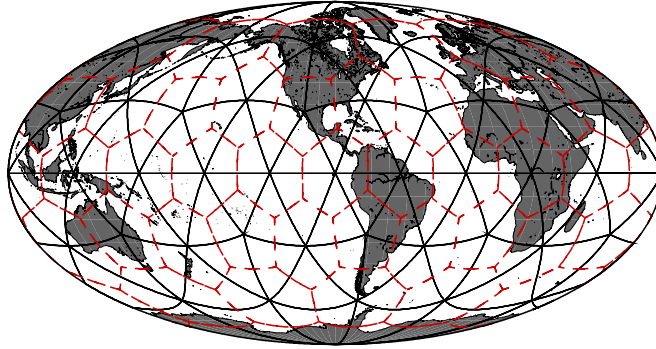


Figure 1: Delaunay and Voronoi grids on the sphere obtained by diadic refinement of the regular icosahedron.

as the intersection between the edges of the Voronoi and Delaunay cells (see figure 1). By construction, each of these points is equidistant from the centers of the Voronoi cells at the ends of that edge. Given the edge  $l$  of a cell, the adjacent cells are denoted by the indexes  $i(l, 1)$  and  $i(l, 2)$ , respectively. The indexes are chosen so that the direction from  $i(l, 1)$  to  $i(l, 2)$  is the positive direction of the normal vector  $\mathbf{N}_l$ . Vertex indexes  $v(l, 1)$  and  $v(l, 2)$  can also be defined analogously, so that the direction from  $v(l, 1)$  to  $v(l, 2)$  is the positive direction of the vector  $\mathbf{T}_l$ .

Given these definitions, discrete operators can be introduced, which will be employed then to define the proposed numerical algorithm. Thanks to the orthogonality between the cell edges and the arcs connecting the cell centers, the directional derivatives in the normal and tangential directions are easily approximated as

$$(\delta_v h)_l = (h_{i(l,2)} - h_{i(l,1)}) / \delta_l, \quad (\delta_\tau h)_l = (h_{v(l,2)} - h_{v(l,1)}) / \lambda_l. \quad (8)$$

Again because of the same orthogonality, discrete divergence and curl operators are now introduced in the context of the C grid staggering outlined above. These operators are defined as acting on a set of values  $g_l$  assigned at the edges of the Voronoi-Delaunay grid. These are to be interpreted as the components of a vector field  $\mathbf{g}_l$  normal to the cell edges, i.e.  $g_l = \mathbf{g}_l \cdot \mathbf{N}_l$ . The discrete divergence and curl operator can be naturally defined as follows:

$$\text{div}(g)_i = \frac{1}{A_i} \sum_{l \in \mathcal{E}(i)} g_l \mathbf{N}_l \cdot \mathbf{n}_{i,l} \lambda_l \quad \text{curl}(g)_v = \frac{1}{A_v} \sum_{l \in \mathcal{E}(v)} g_l \mathbf{N}_l \cdot \mathbf{t}_{v,l} \delta_l. \quad (9)$$

The discrete analogous of the Helmholtz decomposition theorem was proven in [23] for this type of grid arrangement and discrete operators. It should be observed that the velocity points are not equidistant from the adjacent Delaunay grid cell centers. As a result, the difference operators described above are only first order accurate. However, grid optimization procedures such as those introduced in [15] can partly cure this problem and reduce the off-centering to rather small values.

## 4 The numerical method

A basic concept for the horizontal and semi-implicit time discretization of the the Euler equations will be

Level	N. of cells	N. of edges	Av. edge (deg)	Av. $\lambda_l$ (km)	Av. $\delta_l$ (km)
0	20	30	63.43	7053.89	4649.26
1	80	140	33.86	3765.06	2251.11
2	320	480	17.22	1914.39	1017.53
3	1280	1920	8.64	961.26	493.79
4	5120	7680	4.33	481.14	244.99
5	20480	30720	2.17	220.43	122.26
6	81920	122880	1.08	120.32	61.41

Table 1: The triangular icosahedral grid at various resolutions.

presented here in the context of a numerical scheme for the shallow water equations. As customary for the development projects of global models, a prototype based on these simpler equations is being studied as a first step.

The discrete model variables are the velocity components normal to the cell sides and the cell averaged values of the geopotential height, so that the method can be seen as an extension of the C-grid staggering on quadrilateral grids (see e.g. [30]) to triangular grids. The Raviart-Thomas finite element of order zero (see e.g. [24],[25]) is used to reconstruct a uniquely defined velocity field from the velocity components normal to the cell sides. The geopotential gradients, the Coriolis force terms and the divergence of the velocity field are discretized implicitly, while an explicit time discretization is used for the nonlinear advection terms. A preliminary version of the same method was introduced in [5],[6], while its theoretical properties have been extensively analyzed in [7].

The resulting numerical method conserves mass and total vorticity by construction. Results obtained with an implementation on a quasi-uniform icosahedral grid demonstrate the effective accuracy of the proposed method and its potential for application to general circulation models. In most of the approaches developed so far on quasi-uniform spherical grids ([27]), the hexagonal and pentagonal cells of Voronoi tessellations were used as control volumes. However, triangular control volumes allow for much simpler construction of mass conservative models on hierarchies of locally refined grids, along the lines of the cartesian mesh refinement approaches (see e.g. [1], [4], [8]).

Using the notation introduced in section 3, the spatial discretization of the continuity equation (5) is straightforward by integration on cell  $i$  and application of the divergence theorem:

$$\frac{\partial h_i}{\partial t} = -\text{div}(\bar{h}^* u)_i, \quad (10)$$

where  $\bar{h}_i^*$  denotes the arithmetic average of the layer thickness values in the neighbouring cells. The tracer equation (6) can be discretized as

$$\frac{\partial (c_i h_i^*)}{\partial t} = -\text{div}(\bar{c}^* u)_i, \quad (11)$$

where  $\bar{c}$  denotes some reconstructed value of the tracer concentration at the cell edge. A specific choice for the reconstruction method determines a specific advection scheme. For most reconstruction procedures this formulation ensures, by construction, consistency with the discrete continuity equation (10) discussed in section 1, in the sense that setting  $c = 1$  in (6) yields back the discrete continuity equation (10).

The discrete momentum equation can be derived by taking the scalar product of equation (4) with the unit vector  $\mathbf{N}_l$  at a generic velocity point. Using the vector identity

$$(\mathbf{k}_l \times \mathbf{v}) \cdot \mathbf{N}_l = -\mathbf{v} \cdot (\mathbf{k}_l \times \mathbf{N}_l)$$

and the definitions given in the previous section yields the equation

$$\frac{\partial u_l}{\partial t} = -(\bar{\zeta}_l + f_l)v_l - \delta_v \left[ g(h + h^s) + K \right]_l. \quad (12)$$

Here,  $v_l$  is an approximation of the tangential velocity component,  $\zeta_v = \text{curl}(u)_v$  and  $\bar{\zeta}_l$  is the arithmetic average of the absolute vorticity values at the ends of the cell edge. The Raviart-Thomas finite element of order zero (see e.g. [24], [25]) is used to reconstruct at each cell center  $i$  a uniquely defined velocity field from the velocity components normal to the cell sides. The reconstructed vectors from two neighbouring cells are averaged onto the common edge and the tangential component of the resulting vector yields the desired  $v_l$ .

An important feature of this type of spatial discretizations is that, as in the continuous case, taking the discrete curl of equation (12) yields automatically a consistent discretization of the relative vorticity equation. Taking the time derivative of the discrete vorticity one obtains

$$\begin{aligned} \frac{\partial \zeta_v}{\partial t} &= \frac{1}{A_v} \sum_{l \in \mathcal{E}(v)} \frac{\partial u_l}{\partial t} \mathbf{N}_l \cdot \mathbf{t}_{v,l} \delta_l \\ &= \frac{1}{A_v} \sum_{l \in \mathcal{E}(v)} \left[ -(\bar{\zeta}_l + f_l)v_l - \delta_v (gh + K)_l \right] \mathbf{N}_l \cdot \mathbf{t}_{v,l} \delta_l \\ &= -\frac{1}{A_v} \sum_{l \in \mathcal{E}(v)} (\bar{\zeta}_l + f_l)v_l \mathbf{T}_l \cdot \mathbf{n}_{v,l} \delta_l. \end{aligned} \quad (13)$$

Here, the fact that  $\text{curl}(\delta_v \phi_l) = 0$  for any  $\phi_l$  has been used, along with the identity  $\mathbf{N}_l \cdot \mathbf{t}_{v,l} = \mathbf{T}_l \cdot \mathbf{n}_{v,l}$  (see section 3). It can be observed that (13) is indeed a consistent discretization of the vorticity equation (7) on the dual grid cells, where the dual divergence operator can be defined as

$$\text{div}(\psi)_v = \frac{1}{A_v} \sum_{l \in \mathcal{E}(v)} \psi_l \mathbf{T}_l \cdot \mathbf{n}_{v,l} \delta_l.$$

Therefore, the spatial discretization of the momentum equation leads to a vorticity production that corresponds exactly to that implied by the discretization of the equations of motion in vorticity/divergence form. The advantages of this property for finite differences discretizations were highlighted e.g. in [22]. It is to be stressed that the same result can be achieved on any dual Voronoi-Delaunay pair. Staggered grid discretizations on quadrilateral grids also displaying this property have been introduced in [22],[30]. The spatially discretized version of the continuity equation on the dual cells consistent with (12) and (13) can be defined as

$$\frac{\partial h_v}{\partial t} = -\text{div}(\bar{h}^* v)_v, \quad (14)$$

where  $h_v$  is the area weighted average of the values in the triangular cells surrounding vertex  $v$ . Defining the edge averaged potential vorticity values as  $\bar{q} = (\bar{\zeta}_l + f_l)/\bar{h}_l^*$  and using equation (13) leads then to

$$\frac{\partial (q_v h_v^*)}{\partial t} = -\text{div}(\bar{q}^* v)_v, \quad (15)$$

which is the discrete form of potential vorticity conservation that is satisfied by the present method.

A two time level semi-implicit time discretization of equations (4)-(5) is then given by

$$\begin{aligned} u_i^{n+1} &= u_i^n - \Delta t (f_i + \tilde{\zeta}_i^{n+\alpha}) v_i^{n+\alpha} \\ &\quad - \Delta t \left[ \delta_v (gh^{n+\alpha} + \tilde{K}^{n+\alpha}) \right]_i \end{aligned} \quad (16)$$

$$A_i h_i^{n+1} = A_i h_i^n - \Delta t A_i \text{div}(\bar{h}^* u^{n+\alpha})_i. \quad (17)$$

Here,  $\phi^{n+\alpha} = \alpha\phi^{n+1} + (1-\alpha)\phi^n$ ,  $h_l^* = h_l^n - h_l^s$  and  $\alpha \in [\frac{1}{2}, 1]$  for stability, with  $\alpha = \frac{1}{2}$  yielding a second order accurate time discretization in the linear case. On the other hand,  $\tilde{\psi}^{n+\alpha}$  denotes some estimate of the value of  $\psi$  at time  $(n+\alpha)\Delta t$  obtained by an explicit discretization. Along the lines of [22], where a more advanced flux form semi-lagrangian scheme was applied in an analogous step, a simple upwind discretization is employed in this preliminary implementation for these intermediate updates. Since the discrete values of  $\zeta$  are naturally defined at the vertices of the triangular cells, the intermediate update of  $\zeta$  is computed by a discretization using as control volumes the dual hexagonal/pentagonal cells. The value of the tangential velocity component at timestep  $n+1$  can be eliminated by deriving the analog of equation (12) for the tangential velocity component. This yields

$$v_l^{n+1} = v_l^n + \Delta t(f_l + \tilde{\zeta}_l^{n+\alpha})u_l^{n+\alpha} - \Delta t \left[ \delta_\tau(g h^{n+\alpha} + \tilde{K}^{n+\alpha}) \right]_l. \quad (18)$$

Here, the values  $v_l^n$  are to be determined by reconstruction of the full velocity vector at time  $n$  at the velocity node  $l$ . For this reconstruction, the Raviart-Thomas finite element of order zero is employed (see references above) to obtain velocity vectors at the center of each triangular cell, which are then averaged onto the cell edge. The tangential component of the resulting vector yields the desired  $v_l^n$ . The tangential derivative  $\delta_\tau(g h^{n+\alpha} + \tilde{K}^{n+\alpha})_l$  can be approximated by using formula 8, where the values at the vertices are obtained by area weighted averaging. A more accurate, yet still relatively unexpensive approximation of  $\delta_\tau$  is obtained by reconstructing a single discrete gradient vector at the center of each triangular cell via the Raviart-Thomas finite element and subsequently averaging these onto the triangle cell edge, as done in the case of the velocity field. The tangential component of the resulting vector yields the desired approximation of  $\delta_\tau$ . Substituting equation (18) into (16) and then again the resulting expression for  $u_l^{n+1}$  into (17) yields for each cell  $i$  the discrete wave equation

$$\begin{aligned} A_i h_i^{n+1} & - g \alpha^2 \Delta t^2 A_i \operatorname{div} \left[ \left( (\delta_v h^{n+1}) - \alpha \Delta t (f + \tilde{\zeta}^{n+\alpha}) (\delta_\tau h^{n+1}) \right) \gamma h^* \right]_i \\ & = \mathcal{F}_i^n(h), \end{aligned} \quad (19)$$

where one has defined  $\gamma_l = 1/(1 + \alpha^2 \Delta t^2 (f_l + \tilde{\zeta}_l^{n+\alpha})^2)$  and the right hand sides are given by

$$\begin{aligned} \mathcal{F}_i^n(h) & = A_i h_i^n - (1-\alpha) \Delta t A_i \operatorname{div}(h^* u^n)_i - \alpha \Delta t A_i \operatorname{div}(h^* \gamma \mathcal{F}^n(u))_i, \\ \mathcal{F}_i^n(u) & = u_l^n - \Delta t (f_l + \tilde{\zeta}_l^{n+\alpha}) v_l^n - \alpha (1-\alpha) \Delta t^2 (f_l + \tilde{\zeta}_l^{n+\alpha})^2 u_l^n \\ & \quad + \alpha (1-\alpha) \Delta t^2 g (f_l + \tilde{\zeta}_l^{n+\alpha}) \delta_\tau (h^n + \tilde{K}^{n+\alpha})_l \\ & \quad - g (1-\alpha) \Delta t \delta_v (h^n + \tilde{K}^{n+\alpha})_l. \end{aligned}$$

The set of all equations (19) for each cell  $i$  yields a linear system in the unknowns  $h_i^{n+1}$ . Its matrix is sparse and its symmetric part is positive definite and diagonally dominant, which allows for efficient solution even when using relatively simple solvers. Once the values of  $h_i^{n+1}$  have been computed, they are backsubstituted in equation (16) to obtain the final update of the discrete velocities.

## 5 Results of numerical tests

The test cases proposed in the standard shallow water test suite [33] have been run with the currently available implementation. Since no complete normal mode and stability analysis is available so far, no explicit diffusion was employed in our numerical experiments, in order to assess the effective stability and robustness of the proposed method. Values of the implicitness parameter were taken to be in the range [0.55, 0.58].

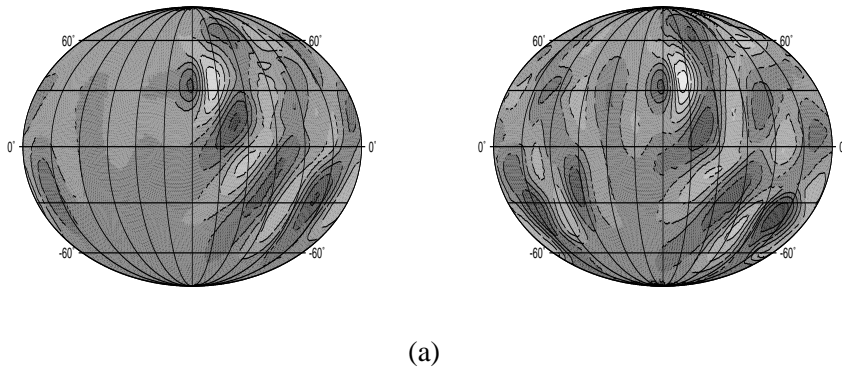


Figure 2: Relative vorticity at day 10 (a) and 15 (b) in Test case 5. Results were computed on grid level 6 with  $\Delta t = 450$  s. Contour lines spacing is  $10^{-5} \text{ s}^{-1}$ .

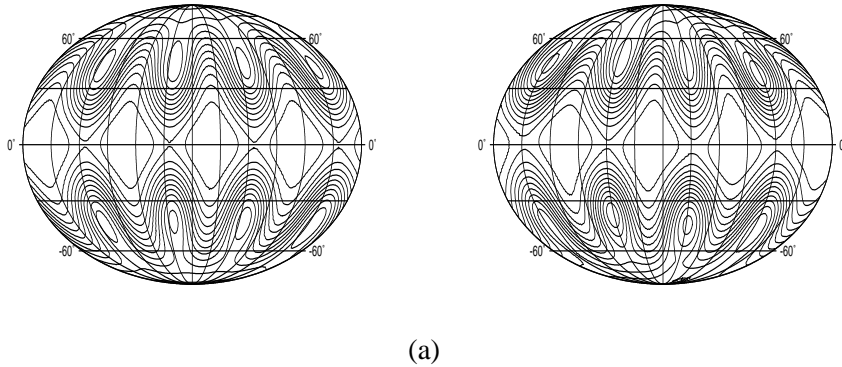


Figure 3: Height field at day 10 (a) and 15 (b) in Test case 6. Results were computed on grid level 6 with  $\Delta t = 225$  s. Contour lines spacing is 100 m.

The correct qualitative behaviour of the computed solutions is shown in figures 2, 3, for test cases 5 and 6, respectively. It should be remarked that the asymmetry developing in the solution of test case 6 on longer time scales is not an indication of inferior performance of the proposed discretization. Indeed, as discussed in [32], the Rossby Haurwitz wave of test 6 is actually unstable as a solution of the shallow water equations. This results in a faster disruption of the wavenumber 4 pattern in all models using grids that are not symmetrical across the equator (see again the comparison presented in [32]).

A full quantitative assessment of the accuracy of the proposed method is presently being undertaken. Only preliminary results are shown here with this respect. For test case 5 a reference solution was obtained with a spectral transform model. For this purpose, the spectral transform model of [18] was revised and upgraded to *fortran90*. The reference solution was computed at spectral resolution of T213 with a timestep of  $\Delta t = 90$ s. In this test, in which a mountain profile with discontinuous derivatives is introduced in a balanced zonal flow at the initial time,  $l_\infty$  convergence can only be achieved away from the mountain. Plots of the height field error at day 15 are shown in figure 4 on grid level 6 and on grid level 7 with  $\Delta t = 900$  s. The results of the corresponding convergence test for the ICON shallow water model are shown in figure 5.

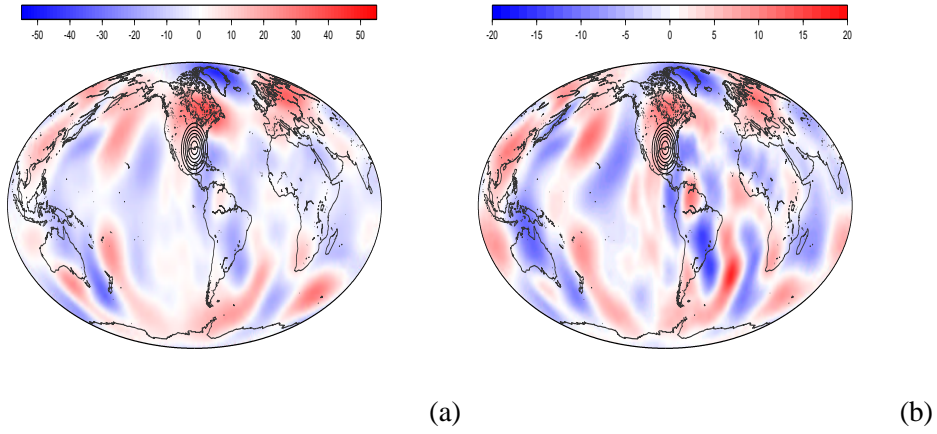


Figure 4: Height field error at day 15 in Test case 5, computed with  $\Delta t = 900$  s on grid level 6 and 7, respectively.

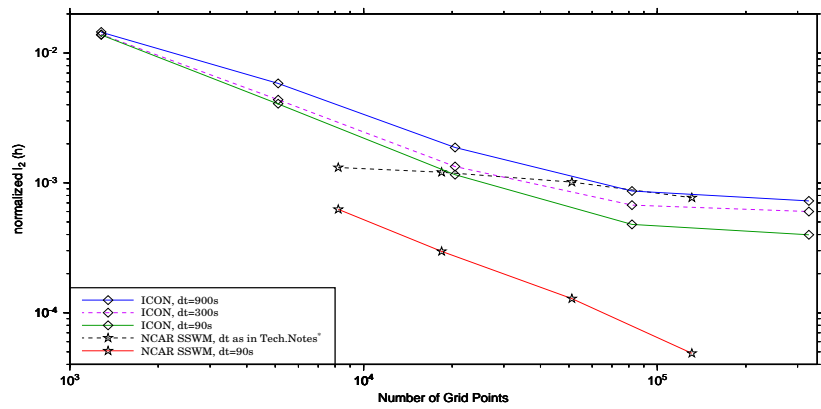


Figure 5: Convergence test for the ICON shallow water model and the reference NCAR spectral transform model.

## 6 Conclusions and future developments

An overview of the ICON project for the development of a nonhydrostatic GCM based on triangular geodesic grids has been presented. The main motivations, targets and features of the new model have been outlined. The horizontal discretization approach has been introduced, in the context of the shallow water model. The resulting numerical method conserves mass and total vorticity by construction. Numerical results obtained with the shallow water model have been presented, showing that the proposed approach allows for accurate simulation of the main features of large scale atmospheric flows.

The evolution of the present model into a full nonhydrostatic GCM will take place in a number of steps. Presently, a multiple resolution version of the shallow water model outlined above is under construction employing the approach introduced in [8] to achieve a mass conservative semi-implicit discretization of the shallow water equations on locally refined icosahedral grids. It is then planned to develop a hydrostatic model using this local grid refinement option, but employing the more standard set of primitive equations and hybrid pressure vertical coordinate as for example in the ECHAM5 model [28], [29]. This will allow to assess the impact of the new horizontal discretization on the existing physical parameterizations and to perform a number of sensitivity studies with respect to the possible local refinements.

## Acknowledgements

I kindly acknowledge the substantial contributions from the whole ICON development team, which also includes Erich Roeckner, Detlev Majewski, Helmut Frank, Marco Giorgetta, Thomas Heinze, Pilar Ripodas, Bodo Ritter and Uwe Schulzweida. In the framework of this project, an extensive and fruitful collaboration with Todd Ringler of Colorado State University, USA has also taken place.

## References

- [1] A. S. Almgren, J.B. Bell, P. Colella, L.Howell, and M.L. Welcome. A conservative adaptive projection method for the variable density incompressible Navier-Stokes equations. *Journal of Computational Physics*, 142:1–46, 1998.
- [2] A. Arakawa and V. Lamb. A potential enstrophy and energy conserving scheme for the shallow water equations. *Monthly Weather Review*, 109:18–136, 1981.
- [3] John R. Baumgardner and Paul O. Frederickson. Icosahedral discretization of the two-sphere. *SIAM Journal of Scientific Computing*, 22(6):1107–1115, December 1985.
- [4] M. J. Berger and P. Colella. Local adaptive grid refinement for shock hydrodynamics. *Journal of Computational Physics*, 82:64–84, 1989.
- [5] L. Bonaventura. Development of the icon dynamical core: modelling strategies and preliminary results. In *Proceedings of the ECMWF/SPARC Workshop on Modelling and Assimilation for the Stratosphere and Tropopause*. ECMWF, 2003.
- [6] L. Bonaventura, L. Kornbluh, T. Heinze, and P. Ripodas. A semi-implicit method conserving mass and potential vorticity for the shallow water equations on the sphere, to appear in. *International Journal of Numerical Methods in Fluids*, 2004.

- [7] L. Bonaventura and T. Ringler. Analysis of discrete shallow water models on geodesic Delaunay grids with C-type staggering, submitted in. *Monthly Weather Review*, 2004.
- [8] L. Bonaventura and G. Rosatti. A cascadic conjugate gradient algorithm for mass conservative, semi-implicit discretization of the shallow water equations on locally refined structured grids. *International Journal of Numerical Methods in Fluids*, 40:217–230, 2002.
- [9] F.A. Bornemann and P. Deuffhard. The cascadic multigrid method for elliptic problems. *Numerische Mathematik*, 75:135–152, 1996.
- [10] M.J.P. Cullen. Integration of the primitive barotropic equations on a sphere using the finite element method. *Quarterly Journal of the Royal Meteorological Society*, 100:555, 1974.
- [11] J. Lili D. Quiang, M. Gunzburger. Voronoi-based finite volume methods, optimal Voronoi meshes and PDEs on the sphere. *Computational Methods in Applied Mechanical Engineering*, 192:3933–3957, 2003.
- [12] M.G. Edwards. Elimination of adaptive grid interface errors in the discrete cell centered pressure equation. *Journal of Computational Physics*, 126:356–372, 1996.
- [13] Francis X. Giraldo. Lagrange-Galerkin methods on spherical geodesic grids: The shallow water equations. *Journal of Computational Physics*, 160:336–368, 2000.
- [14] E.S. Gross, L. Bonaventura, and G. Rosatti. Consistency with continuity in conservative advection schemes for free-surface models. *International Journal of Numerical Methods in Fluids*, 38:307–327, 2002.
- [15] Ross Heikes and David A. Randall. Numerical integration of the shallow-water equations on a twisted icosahedral grid. Part II: A detailed description of the grid and an analysis of numerical accuracy. *Monthly Weather Review*, 123:1881–1887, June 1995.
- [16] Ross Heikes and David R. Randall. Numerical integration of the shallow-water equations on a twisted icosahedral grid. Part I: Basic design and results of tests. *Monthly Weather Review*, 123:1862–1880, June 1995.
- [17] T. Heinze and A. Hense. The shallow water equations on the sphere and their Lagrange-Galerkin solution. *Meteorology and Atmospheric Physics*, 81:129–137, 2002.
- [18] Ruediger Jakob-Chien, James J. Hack, and David L. Williamson. Spectral transform solutions to the shallow water test set. *Journal of Computational Physics*, 119:164–187, 1995.
- [19] P. Jöckel, R. von Kuhlmann, M.G. Lawrence, B. Steil, C.A.M. Brenninkmeijer, P.J. Crutzen, P.J. Rasch, and B. Eaton. On a fundamental problem in implementing flux-form advection schemes for tracer transport in 3-dimensional general circulation and chemistry transport models. *Quarterly Journal of the Royal Meteorological Society*, 127:1035–1052, 2001.
- [20] Randall J. Leveque. High-resolution conservative algorithms for advection in incompressible flow. *SIAM Journal of Scientific Computing*, 33(2):627–665, April 1996.
- [21] Shian-Jiann Lin and Richard B. Rood. Multidimensional flux-form semi-Lagrangian transport schemes. *Monthly Weather Review*, 124:2046–2070, September 1996.
- [22] Shian-Jiann Lin and Richard B. Rood. An explicit flux-form semi-Lagrangian shallow water model on the sphere. *Quarterly Journal of the Royal Meteorological Society*, 123:2477–2498, 1997.

- [23] R.A. Nicolaides. Direct discretization of planar div-curl problems. *SIAM Journal of Numerical Analysis*, 29:32–56, 1992.
- [24] Alfio Quarteroni and Alberto Valli. *Numerical approximation of partial differential equations*, chapter 9: The Stokes problem. Springer Verlag, 1994.
- [25] P.A. Raviart and J.M. Thomas. A mixed finite element method for 2nd order elliptic problems. In *Mathematical aspects of finite element methods.*, pages 292–315. Springer Verlag, Lecture Notes in Mathematics, I. Galligani and E. Magenes eds. 1977.
- [26] Todd D. Ringler, Ross P. Heikes, and David A. Randall. Modeling the atmospheric general circulation using a spherical geodesic grid: A new class of dynamical cores. *Monthly Weather Review*, 128:2471–2490, July 2000.
- [27] Todd D. Ringler and David A. Randall. A potential enstrophy and energy conserving numerical scheme for solution of the shallow-water equations a geodesic grid. *Monthly Weather Review*, 130:1397–1410, July 2002.
- [28] E. Roeckner, G. Bäuml, L. Bonaventura, R. Brokopf, M. Esch, M. Giorgetta, S. Hagemann, I. Kirchner, L. Kornblueh, E. Manzini, A. Rhodin, U. Schlese, U. Schulzweida, and A. Tompkins. The atmospheric general circulation model ECHAM 5. PART I: model description. MPI Technical Report 349, MPIM, 2003.
- [29] E. Roeckner, R. Brokopf, M. Esch, M. Giorgetta, S. Hagemann, I. Kirchner, L. Kornblueh, E. Manzini, A. Rhodin, U. Schlese, U. Schulzweida, and A. Tompkins. The atmospheric general circulation model ECHAM 5. PART II: Sensitivity of simulated climate to horizontal and vertical resolution. MPI Technical Report 354, MPIM, 2004.
- [30] R. Sadourny. The dynamics of finite difference models of the shallow water equations. *Journal of the Atmospheric Sciences*, 32:680–689, 1975.
- [31] C. Schär and P.K. Smolarkiewicz. A synchronous and iterative flux-correction formalism for coupled transport. *Journal of Computational Physics*, 128:101–120, 1996.
- [32] J. Thuburn and Y. Li. Numerical simulation of Rossby-Haurwitz waves. *Tellus A*, 52:181–189, 2000.
- [33] David L. Williamson, John B. Drake, James J. Hack, Rüdiger Jakob, and Raul N. Swarztrauber. A standard test set for numerical approximations to the shallow water equations in spherical geometry. *Journal of Computational Physics*, 102:221–224, 1992.